Supporting Information

Efficient Exciton Dissociation and Harvesting for the Sacrificial Agent and ROS-Free Simultaneous Photoredox Removal of Uranium(VI) by e^- and Ciprofloxacin by h^+ Using Triazine-based CMPs

Suman Karmakar[a,#], Soumitra Sau[a,#], Shubhangi Majumdar[b], Pramit K. Chowdhury[b] and Suman Kalyan Samanta[a,*]

[a]Department of Chemistry, Indian Institute of Technology Kharagpur, Kharagpur 721302, India. E-mail: sksamanta@chem.iitkgp.ac.in

[b]Department of Chemistry, Indian Institute of Technology Delhi, New Delhi 110016, India

1. Experimental Section

1.1. Materials and Methods. Solvents were dried prior to use in accordance with standard procedures. Thin layer chromatography (TLC) on silica gel GF254 was used for the determination of R_f values and the visualization was performed by irradiation with UV lamp at 254 nm. Column chromatography was performed on Merck silica gel (100-200 mesh) with eluent as mentioned. ^{1}H (500 MHz) and ^{13}C (125 MHz) NMR spectra were recorded in a Bruker advance-500 NMR spectrometer in deuterated solvent at ambient temperature (300 K). Chemical shifts are reported in ppm (δ) relative to tetramethylsilane (TMS) as the internal standard ($CDCl_3$ δ 7.26 ppm for ^{1}H and 77.0 ppm for ^{13}C). Solid state ^{13}C CPMAS NMR spectra were recorded in a Bruker Ultrashield-500 NMR spectrometer. Fourier transform infrared spectra (FTIR, 4000-600 cm^{-1}) were performed on Nicolet 6700 FT-IR spectrometer (Thermo Fischer) instrument, the wave numbers of recorded IR-signals are reported in cm^{-1}. Thermogravimetric analyses (TGA) were performed on a Pyris Diamond TG DTA (PerkinElmer) instrument. The as synthesized D-A CMPs were observed under scanning electron microscope (SEM) model ZEISS SUPRA 40. The samples were prepared on gold stubs by adding powder polymers mounting on top of double-sided tapes. UV-Vis-NIR diffuse reflection spectrum (DRS) was acquired with UV-vis-NIR spectrophotometer (Cary 5000, Agilent). X-Ray diffraction patterns of the powder organic polymer samples were obtained using a Bruker AXS D-8Advanced SWAX diffractometer using Cu-Kα (0.15406 nm) radiation. The N_2 adsorption/desorption isotherms of the sample was recorded on a Quantachrome Autosorb iQ2 at 77 K. UV-visible absorption spectra were recorded on a Shimadzu UV-2550 UV-Vis spectrophotometer. Then the polymer was filtered out and the filtrate portion was submitted for UV. Bruker ELEXSYS 580 spectrometer was used to record the EPR spectra. Ultrafast transient absorption measurements were conducted using a commercial one-box ultrafast Ti: Sapphire amplifier (Astrella 1K-F, 100 fs, 5 mJ/pulse, and 1 kHz repetition rate, Coherent Inc.,) with an integrated oscillator (Vitara-S, 400 mW at 800 nm, 70 nm bandwidth, pumped by Verdi-G, 80 MHz) and coupled to a femtosecond transient absorption spectrometer (Helios Fire UV-VIS, Ultrafast Systems). The amplified output (5mJ/pulse, 1 kHz) of central wavelength 800 nm was divided into two parts. One part (~200 mW) was used to produce the femtosecond probe pulse by focusing it either on a CaF_2 (for UV probe: 310 – 615 nm) or 2-mm thick sapphire crystal for white light continuum (400-800 nm) while the other part (3.25 mW) was used to generate a tunable femtosecond pump pulse using an optical parametric amplifier (OPerA Solo, 290 – 2600 nm). After the sample, the probe beam (1 kHz) was collimated and then focused into a fiber-optics coupled multichannel spectrometer equipped with CMOS sensor (1024 pixels). The pump power used in the experiment was controlled by a variable neutral-density filter wheel and kept at ~0.5 mW. Both the pump and probe beams overlapped at the sample cuvette and the delay between the pump and probe pulses was controlled by a motorized delay stage. The pump pulses were chopped by a synchronized chopper at 500 Hz and the absorbance change was calculated with two adjacent probe pulses (pump-blocked and pump-unblocked). TOC measurements were performed using a Shimadzu TOC-VCPH analyzer. Temperature-dependent photoluminescence (PL) spectra were recorded using a PicoQuant Fluo Time-300 spectrometer.

1.2. TAS Experiments:

The samples dispersed in DMF (O.D. kept at 0.8 in 1cm quartz cuvette) were held in a 2 mm quartz cuvette containing a magnetic bead inside and stirred constantly by a magnetic stirrer during the measurements to minimize photodamage. For transient measurements, 350 nm was used as the pump wavelength, and a sapphire crystal was used to generate white light continuum (400 – 700 nm) for probing the visible range. To check for any photodamage to the sample during transient absorption measurements, ground-state absorption spectra were taken before and after the completion of the experiments, with no change in spectra observed. Surface Xplorer version 4.5 was used to analyze the transient absorption spectra.

Calculations of Decay Time:

The transient decays were fitted by equation (1), using an IRF of ~150 fs with the help of Surface Xplorer software and the average lifetimes were calculated according to equation (2). $\Delta A\ (\lambda, t)$ is the observed change in absorbance at time t and wavelength λ, A is amplitude and τ is the time constant of i^{th} component.

$$\Delta A\ (\lambda, t) = A_0 + \sum_i A_i\, e^{-\frac{t}{\tau_i}} \qquad (1)$$

$$< \tau >= \frac{\sum_i A_i \tau_i}{\sum_i A_i} \qquad (2)$$

1.2. Calculation for VB XPS: The results obtained for valence band offset (VB_{xps}) of **TRZ-AQ** and **TRZ-PHQ** are 2.19 eV and 1.68 eV respectively. The electron work function (Φ) of the analyzer was 4.35 eV. Using these values in equation (S1), the valence band potential could be obtained[1]

$$E_{VB} = \Phi + VB\ xps - 4.44 \qquad (S1)$$

1.3. Electrochemical measurements

Cyclic voltammetry (CV) measurement was carried out by using a CH instrument with a three electrode-cell [CMPs-coated glassy carbon electrode as a working electrode, platinum wire as a counter electrode, and Ag/Ag^+ in acetonitrile (+0.49 V vs NHE)[2] as a reference electrode. A scan rate of 0.1 V/s was used. A solution of 0.1 (M) tetrabutylammonium hexafluorophosphate in acetonitrile was used as the supporting electrolyte. 2 mg of well-dried POPs was well dispersed in a binder solution of 25 wt% of polyvinylidene fluoride (PVDF) and 500 µL of ethanol through ultrasonication for 1 h to obtain a stable suspension. Then the pre-polished glassy carbon electrode was coated by 20 µL of the prepared polymeric dispersion. The electrode was dried for 1 day at room temperature and then prior to CV experiment. The

electrode potential values are given with respect to $E_{Ag/AgCl}$ = 0.197 vs NHE.[3] The LUMO energy levels of the POPs were determined by using the empirical equations, E_{LUMO} = ($E_{onset/red}$+0.49-0.197)V (vs Ag/AgCl).[4, 5] EIS was determined over the frequency range of 10^2–10^6 Hz with an ac amplitude of 10 mV at the open circuit voltage under room-light illumination by using 0.5 M Na_2SO_4 aqueous solution as supporting electrolyte.

1.4. Photoelectrochemical measurements

Photoelectrochemical measurements were conducted in a three-electrode system using CH instrument under 20 W white LED. The working electrodes are prepared as follows: 2 mg of well-dried CMPs is separately ground with 0.5 mg of polyvinylidene fluoride (PVDF) and 50 µL of ethanol to make slurry. The slurry is then coated onto FTO glass electrodes with an active area of 1 cm^2, and these electrolytes were dried at 80 °C for 1 h to evaporate the solvent. An aqueous solution of 0.5 M Na_2SO_4 was used as the supporting electrolyte. Photocurrent measurements and Mott–Schottky analysis were carried out using the CMP-coated FTO as the working electrode, a platinum wire as the counter electrode, and an Ag/AgCl (3 M KCl) electrode as the reference. Transient photocurrent responses were measured at 0.3 V versus Ag/AgCl under chopped light illumination. Flat-band potentials (vs. Ag/AgCl) were determined from the extrapolated tangent of the Mott–Schottky plots collected at frequencies of 1250, 1500, and 1750 Hz.

1.5. Determination of Quantum Yield:

Determination of the photon flux (I_0): Photon flux from the incident light source was quantitatively determined via chemical actinometry using indolyl fulgide, following the protocol established by Mondal et al.[6] The fundamental photochemical mechanism underlying fulgide-based actinometry is depicted below-

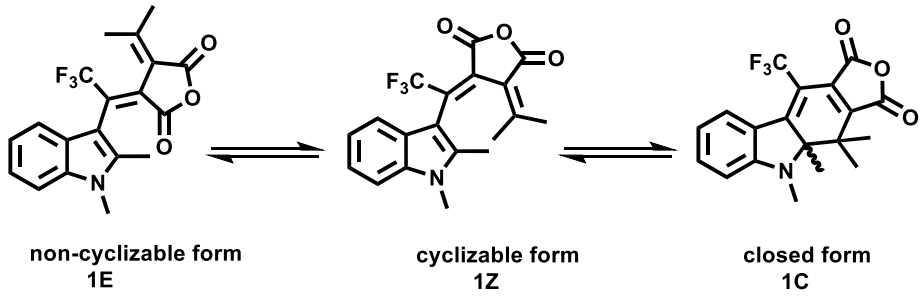

A freshly prepared solution of compound 1 (3 ml, 1.0×10^{-4} M) in toluene was transferred to a fluorescence cuvette containing a magnetic stir bar to ensure homogeneity during irradiation. The temporal evolution of the absorption spectra was recorded by monitoring the change in absorbance at 427 nm, expressed as ($A_0 - A$) versus irradiation time (t). The photon flux associated with the photoisomerization of the 1Z isomer to the 1C isomer was quantified using

Equation 1.[7] This photon flux was subsequently utilized to determine the photochemical quantum yield of the reaction.

$$I_0 = \frac{\Delta A}{t}\frac{V}{\varepsilon d \Phi} \quad \ldots\ldots\ldots\ldots\ldots\ldots (1)$$

Where 'I_0' represents the photon flux of the incident light (Einsteins.s^{-1}), 'ΔA' denotes the growth of the closed form (1C) in time 't,' 'V' is the sample volume (mL), 'ε' is the molar absorption coefficient of the 1Z isomer at 427 nm ($M^{-1}.cm^{-1}$), 'd' is the optical path length of the cuvette (cm), and 'Φ' is the quantum yield of the photoisomerization reaction.

(a) UV-vis spectral changes of the indolyl fulgide under blue light irradiation (456 ± 10 nm) and (b) the time-dependent absorbance changes monitored at 427 nm are shown below-

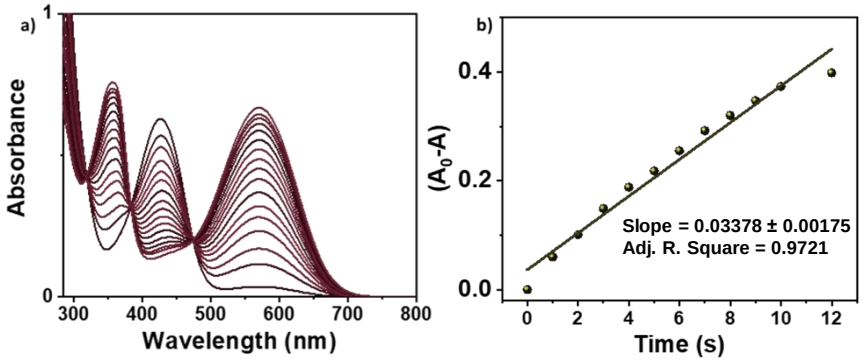

Incident Light	Slope (ΔA/t)	Sample Volume (cm^3)	Photon Flux (Einstein s^{-1})
456 ± 10 nm	0.03378 ± 0.00175	3	2.05×10^{-7}

Determination of the apparent quantum yield (AQY):

Apparent quantum yield (Φ) of the photochemical reaction was determined using equation (2)

$$\mathbf{AQY} = \frac{\Delta C \times V}{Flux \times t} \quad \ldots\ldots\ldots\ldots\ldots\ldots\ldots\ldots (2)$$

Where, ΔC represents the change in concentration (mol L^{-1}), V is the solution volume (L), t is the reaction time (s), and Flux denotes the incident photon flux (Einstein s^{-1}).

1.5.1 Determination of AQY for the photocatalytic removal of Uranium(VI) in presence of CIP (50 ppm):

$$U(VI) \xrightarrow[140\ min,\ 94\%]{TRZ\text{-}PHQ} U(IV)$$

$$\Phi = \frac{0.094\ \times 10^{-3}\ mol.L^{-1} \times 0.01\ L}{2.05 \times 10^{-7}\ E.s^{-1} \times (140 \times 60)s} \times\ 100 = 0.054$$

1.5.2. Determination of AQY for the photocatalytic degradation of CIP under simultaneous reaction conditions:

$$Ciprofloxacin \xrightarrow[140\ min,\ 79\%]{TRZ\text{-}PHQ} Degradation\ products$$

$$\Phi = \frac{0.12\ \times 10^{-3}\ mol.L^{-1} \times 0.01\ L}{2.05 \times 10^{-7}\ E.s^{-1} \times (140 \times 60)s} \times\ 100 = 0.070$$

1.5.3. Determination of AQY for the photocatalytic removal of Uranium(VI) in presence of CIP (150 ppm):

$$U(VI) \xrightarrow[40\ min,\ 88\%]{TRZ\text{-}PHQ} U(IV)$$

$$\Phi = \frac{0.087\ \times 10^{-3}\ mol.L^{-1} \times 0.01\ L}{2.05 \times 10^{-7}\ E.s^{-1} \times (40 \times 60)s} \times\ 100 = 0.18$$

2. Characterization:

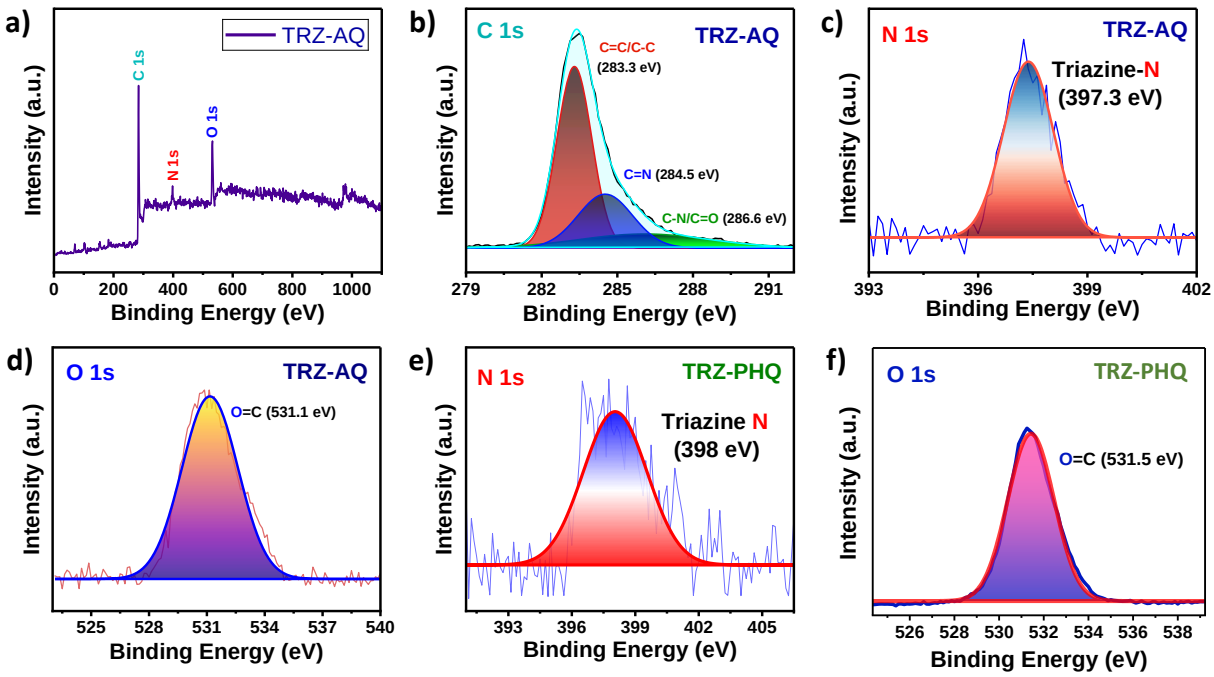

Figure S1. a) Full-range XPS spectrum of **TRZ-AQ;** high-resolution deconvoluted XPS spectra of b) C 1s, c) N 1s and d) O 1s for **TRZ-AQ**; and e) N 1s, f) O 1s for **TRZ-PHQ**.

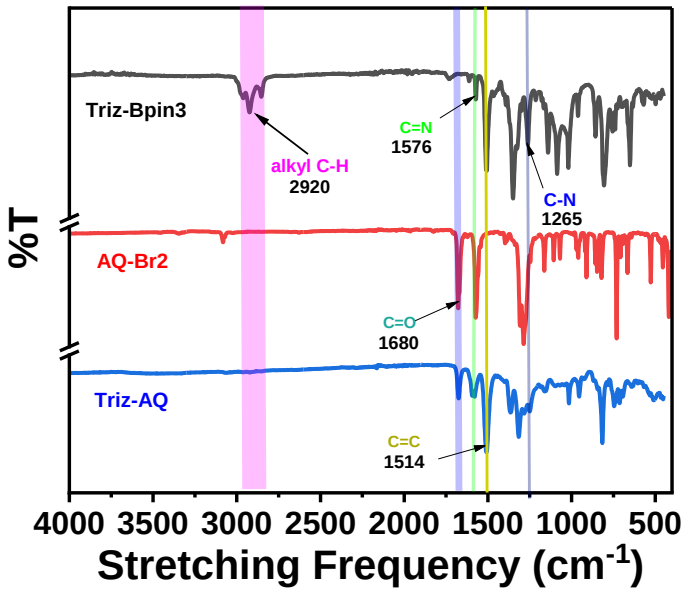

Figure S2. FT-IR spectra of monomer AQ-Br2 (red), monomer TRZ-Bpin3 (black) and polymer **TRZ-AQ** (blue).

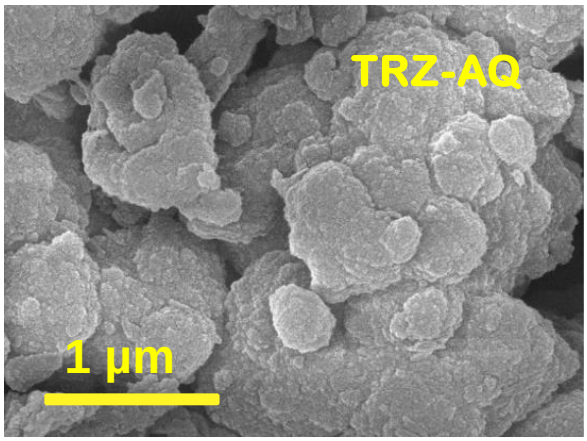

Figure S3. SEM image of **TRZ-AQ**.

a)

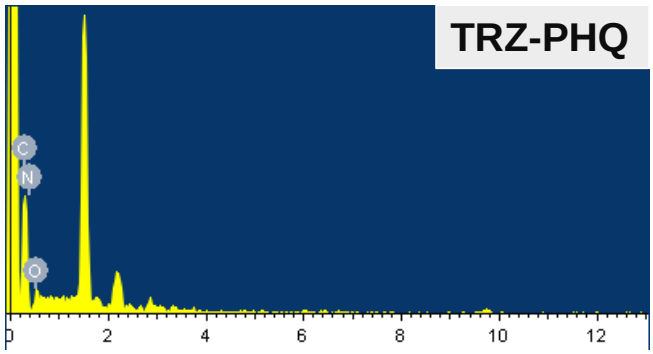

Element	Weight %	Atomic %
C K	65.42	70.39
N K	14.67	13.53
O K	19.91	16.08

b)

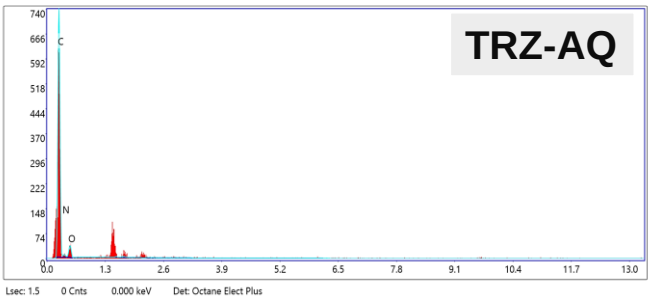

Element	Weight %	Atomic %
C K	88.78	90.99
N K	3.46	3.04
O K	7.77	5.98

Figure S4. Energy dispersive X-ray (EDX) analysis of a) **TRZ-PHQ** and b) **TRZ-AQ**; inset: tabular representation of different elements in atomic % and weight % present in the polymer.

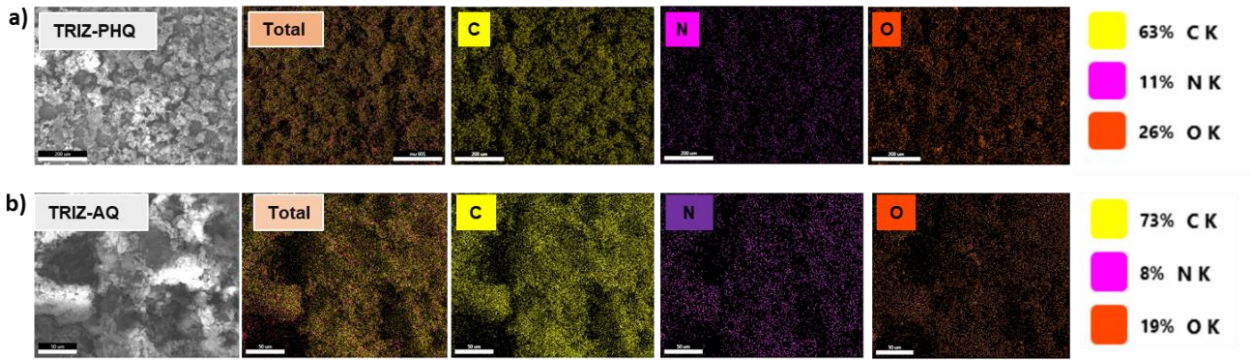

Figure S5. Elemental mapping analysis of a) **TRZ-PHQ** and b) **TRZ-AQ**.

Table S1. BET surface area, pore size and pore volume of the CMPs.

SL. No.	Sample Name	BET Surface area	Pore size (nm)	Pore Volume (cc/g)
1	**TRZ-AQ**	43	0.7	0.087
2	**TRZ-PHQ**	53	1.32	0.124

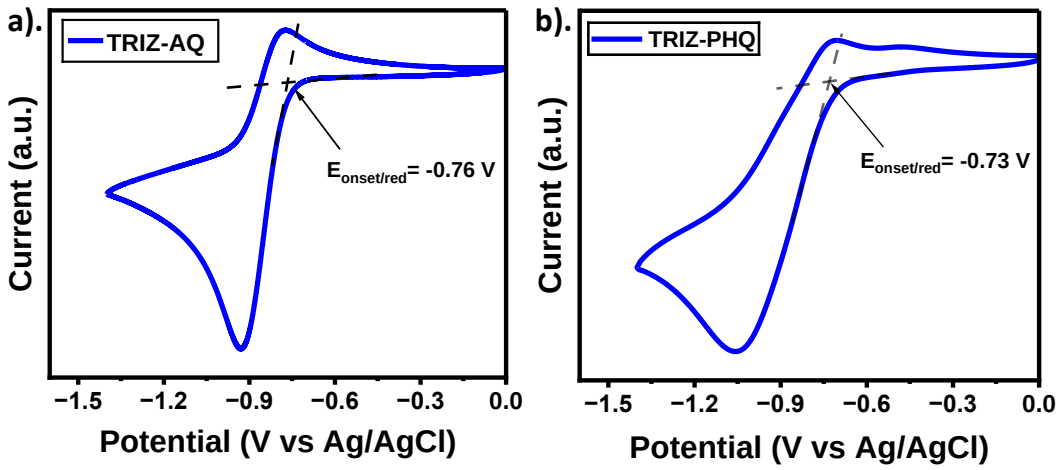

Figure S6. CV plots of **TRZ-AQ** and **TRZ-PHQ**.

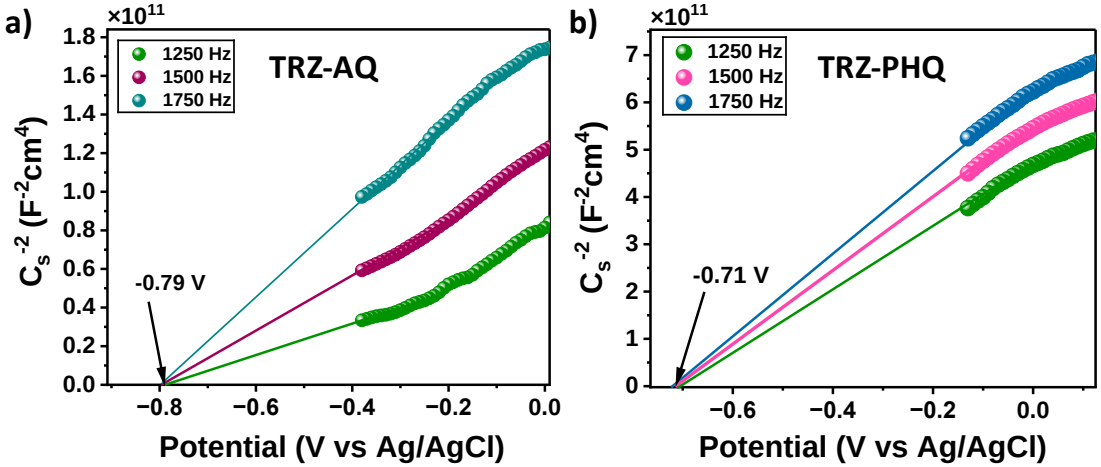

Figure S7. Mott–Schottky plots of a) **TRZ-AQ** and b) **TRZ-PHQ** recorded at three different frequencies.

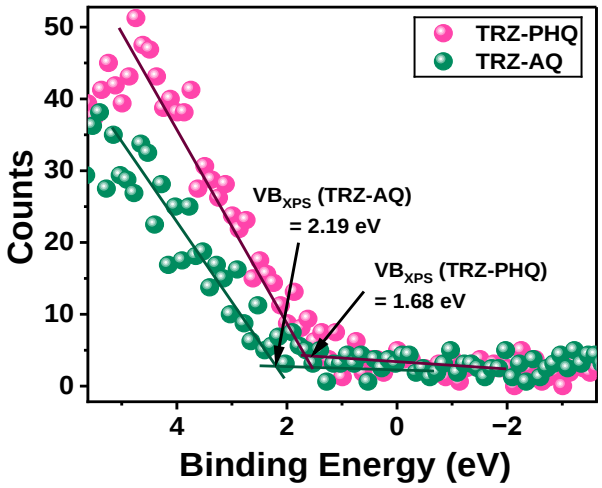

Figure S8. Valence band XPS spectra of the CMPs.

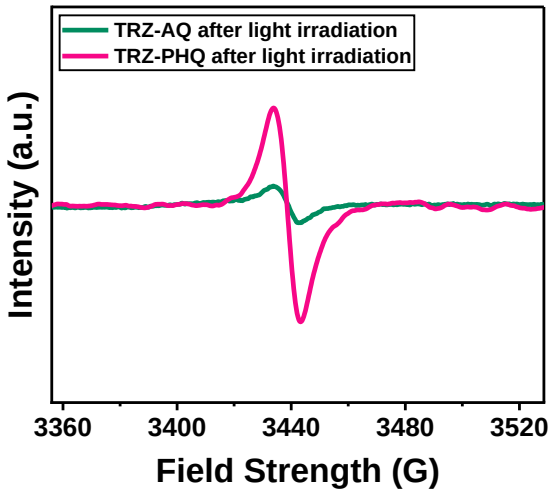

Figure S9. EPR spectra of the CMPs under visible-light irradiation;

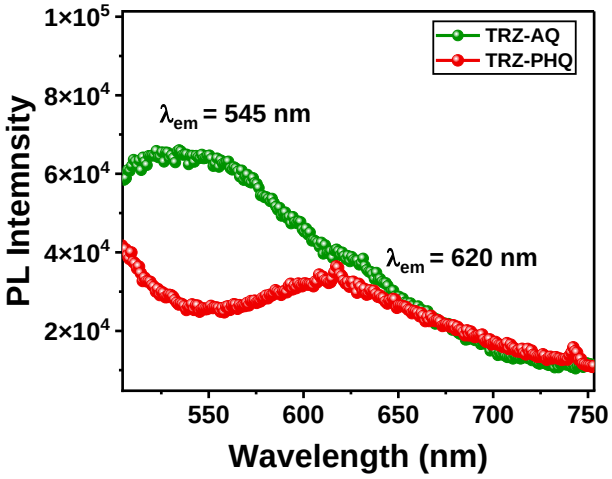

Figure S10. steady-state PL spectra of the CMPs.

Table S2. Simulated R_s and R_{ct} values of CMPs for electrochemical impedance test

Sample	R_s/Ω	$R_{ct}/k\Omega$
TRZ-PHQ	13.6	8.9
TRZ-AQ	13.5	17.6

In the equivalent circuit (inset, Figure 2g) , R_s represents the circuit series-resistance, CPE is the capacitance phase element of the semiconductor-electrolyte interface, and R_{ct} is the charge transfer resistance across the interface.

TAS Experiments: To correlate the transient absorption studies with the broad excitation window of the photocatalytic setup, additional measurements were performed at 450 and 550 nm (Figure S11). The kinetics of **TRZ-PHQ** under nitrogen environment upon 450 nm excitation closely match those obtained at 350 nm, confirming that the essential relaxation dynamics are preserved under visible excitation. In contrast, both **TRZ-PHQ** and **TRZ-AQ** showed no excited-state absorption upon 550 nm excitation, indicating that this wavelength does not effectively populate the reactive states.

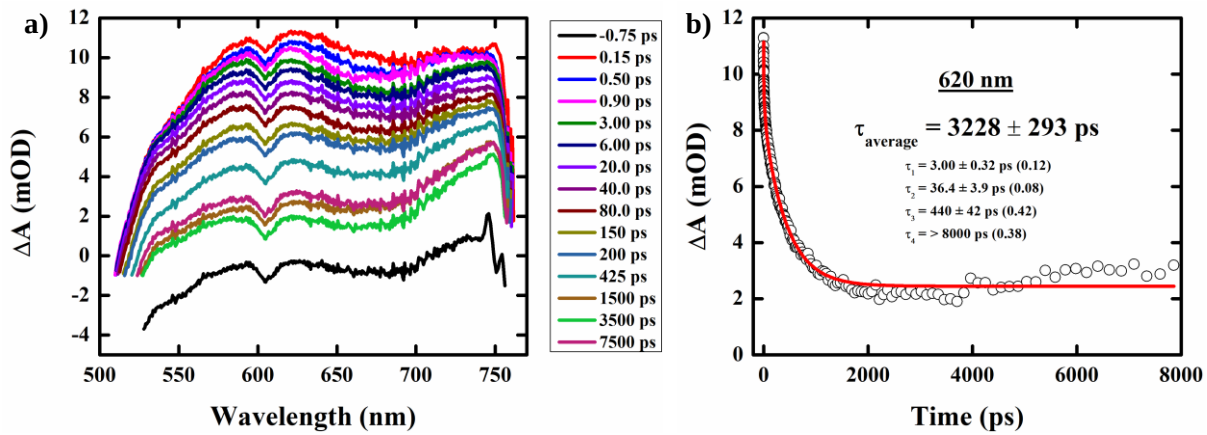

Figure S11: a) Transient absorption spectra, b) Single wavelength kinetics, probing at 620 nm of **TRZ-PHQ** in nitrogen atmosphere, exciting at 450 nm.

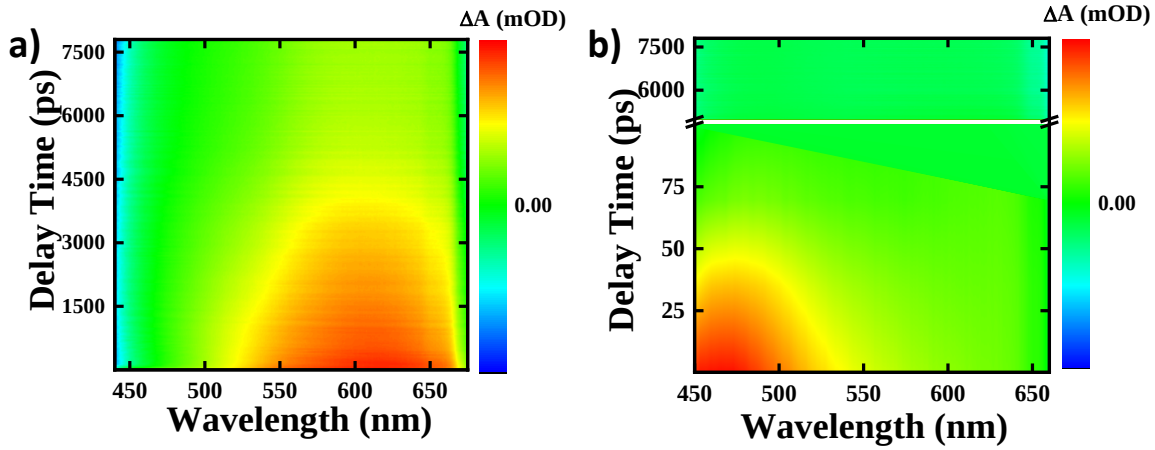

Figure S12. Contour plots for the transient absorption spectra of a) **TRZ-PHQ** and b) **TRZ-AQ**.

3. Photocatalytic Application

3.1. Photocatalytic Uranium extraction studies

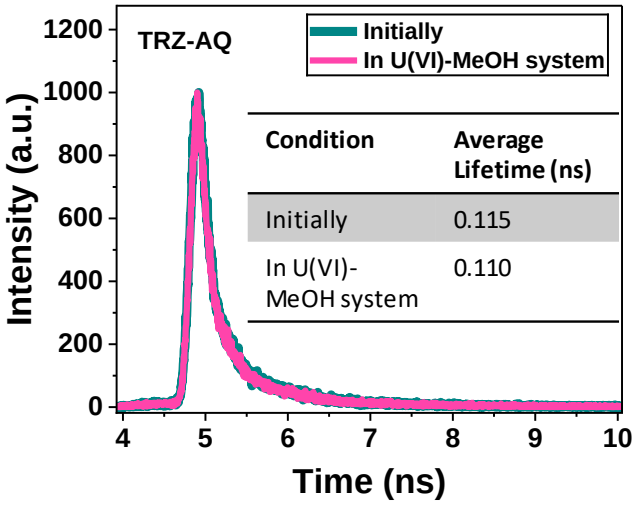

Figure S13. TRPL spectra of **TRZ-AQ** in aqueous and U(VI)-MeOH system.

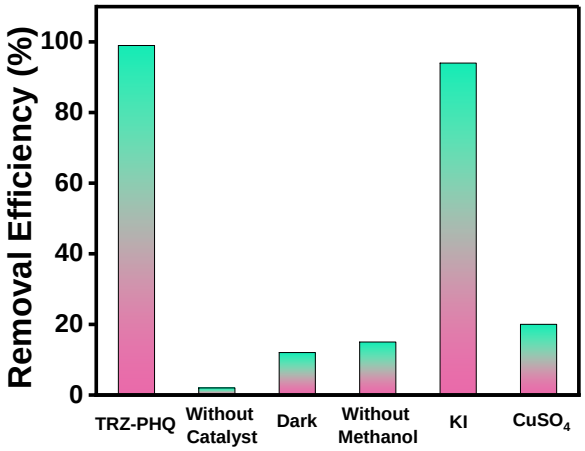

Figure S14. Control tests for photocatalytic reduction of uranium by **TRZ-PHQ.**

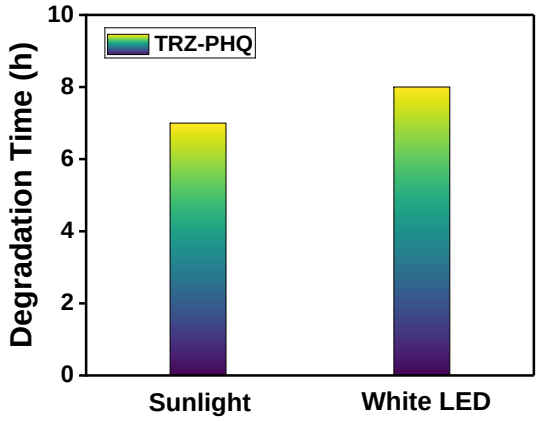

Figure S15. Degradation time on photocatalytic removal of uranium for **TRZ-PHQ** under sunlight and white LED.

Table S3. Comparison of photocatalytic removal capacities of U(VI) on various photocatalysts.

Material type	Photocatalyst	Solid to liquid ratio	Photocatalytic conditions	pH	q_e (mg g^{-1})	Ref.
Polymer	TRZ-PHQ	0.2 g L^{-1}	Methanol, 50 ppm	7.0	1240	This work
	PQ-TPM	0.125 g L^{-1}	Methanol, 50 ppm	4.0	2024.9	8
	TiO_2	0.4 g L^{-1}	HCOONa, 50 ppm	5.5	221	9
	g-C_3N_4	0.2 g L^{-1}	Methanol, 50 ppm	5.0	241	10
	g-C_3N_4/TiO_2	0.25 g L^{-1}	NA, 20 ppm	6.9	66.4	11
	CN550	0.2 g L^{-1}	Methanol 2mL, 326.5 ppm	6.0	1556	12
	Ti_3C_2/CdS	0.2 g L^{-1}	200 ppm	8.5	500	13
	PyB-SO_3H	0.2 g L^{-1}	Methanol, 50 ppm	4.0	211.26	14
COF	NDA-TN-AO	0.005g/L	10 ppm	5.0	589.1	15
	SnS_2COF	0.5 g/L	550 ppm	5.0	1123.3	16
	PyN-DAB	0.143 g/L	600 ppm	4.0	1436.4	17
	BiOBr@TpPa-1	0.33 g L^{-1}	Methanol, 50ppm	2-7	81.9	18
	Tp-DBD	0.01g/L	35 ppm	6.0	1006.5	19
	BD-TN-AO	0.25g/L	20 ppm	5.0	562	20
MOF	PN-PCN-222	0.5 g L^{-1}	Methanol, 400 ppm	3.0-11.0	1289	21
	Cu SA@UiO-66-NH_2	0.005	8 ppm	6.0	284.09	22
	SCN-19	0.5 g L^{-1}	400 ppm	4.0	625	23
	ZIF-8/C_3N_4	0.1 g L^{-1}	10 ppm	4-8	100	24

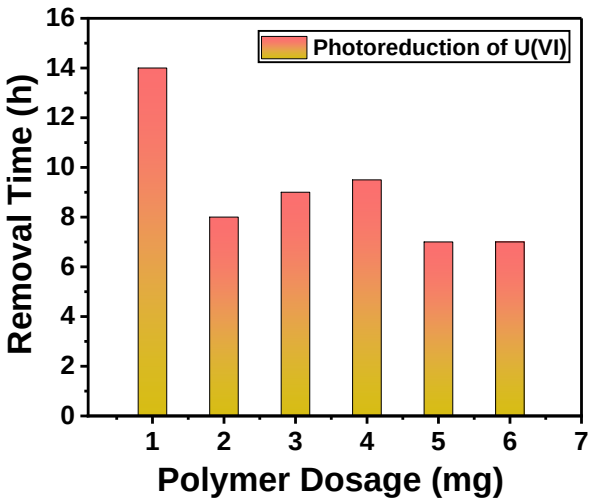

Figure S16. Optimization of polymer dosage in photoreduction of U(VI), at pH = 7.0.

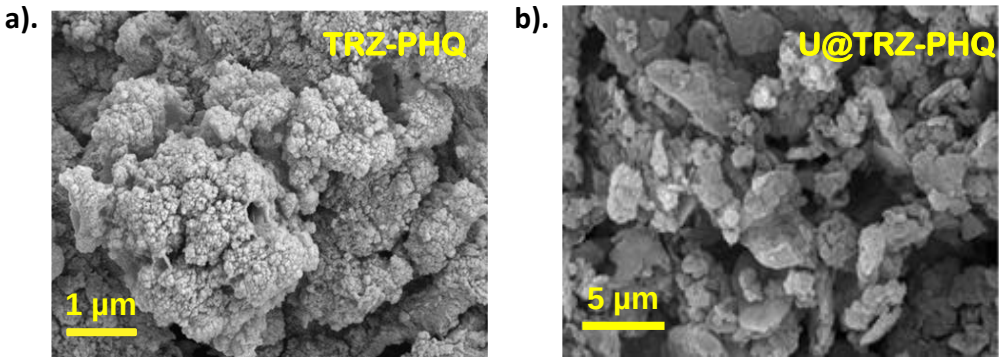

Figure S17. FE-SEM images of **TRZ-PHQ** a) before and b) after photocatalytic removal of U(VI).

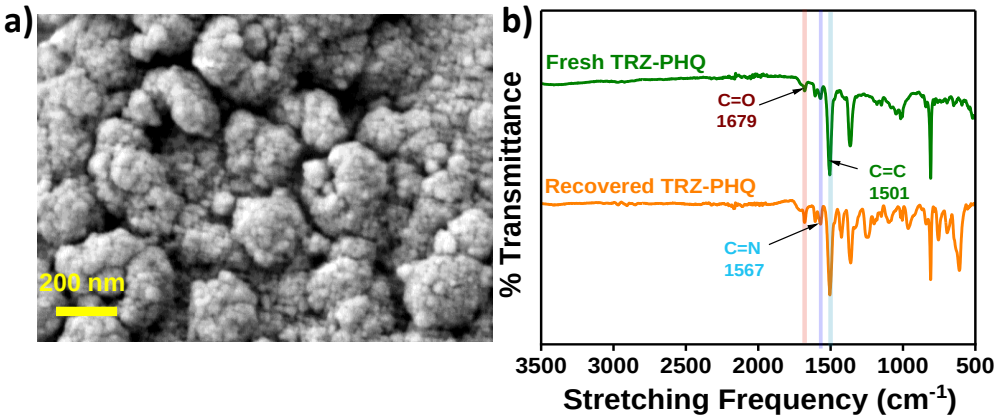

Figure S18. a) SEM image of recovered **TRZ-PHQ** after 5th cycle; b) FTIR spectra of fresh **TRZ-PHQ** and recovered **TRZ-PHQ** after 5th cycle.

Table S4. The percentages of photodegradation of CIP by other photocatalysts in literature.

Photocatalyst	Conc. (mg/L)	Dosage (g/L)	Time (min)	Removal efficiency (%)	Rate constant	Light source	Ref.
TRZ-PHQ	20	0.5	360	91	0.42 h^{-1} (0.007 min^{-1})	100 W LED ($\lambda \geq 400$ nm)	This work
Polypyrrole/zinc ferrite/g-C_3N_4	20	1.0	120	92	0.0215 min^{-1}	300 W XL ($\lambda \geq 420$ nm	25
Ternary sepiolite/g-C_3N_4/Pd	10	0.4	60	64	0.0166 min^{-1}	500 W XL ($\lambda \geq 380$ nm)	26
Porous defect g-C_3N_4	10	1.0	120	78	……	300 W XL ($\lambda \geq 420$ nm)	27
Oxygen-doped porous g-C_3N_4	10	1.0	20	95	0.122 min^{-1}	500 W XL ($\lambda \geq 380$ nm)	28
pCdS/Cu_2O/g-C_3N_4	20	0.025	150	99	0.030 min^{-1}	300 W XL ($\lambda \geq 420$ nm)	29
Fe-MOF@BiOBr/M-CN	10	0.625	120	93	0.01645 min^{-1}	300 W XL ($\lambda \geq 420$ nm)	30
g-C_3N_4/RGO/WO_3	20	0.2	180	85	…….	500 W XL ($\lambda \geq 400$ nm)	31
g-C_3N_4/Ti_3C_2	20	0.2	150	100	0.035 min^{-1}	500 W XL ($\lambda \geq 400$ nm)	32
g-C_3N_4/α-Fe_2O_3/Bi_3TaO_7	5	0.2	120	95.6	0.0239 min^{-1}	500 W XL ($\lambda \geq 420$ nm)	33
BiOBr/CDs/g-C_3N_4	10	0.65	105	83.4	0.01797 min^{-1}	300 W XL ($\lambda \geq 420$ nm)	34
3B-PCN	10	0.4	60	87.56	0.01151 min^{-1}	300 W XL ($\lambda \geq 420$ nm)	35

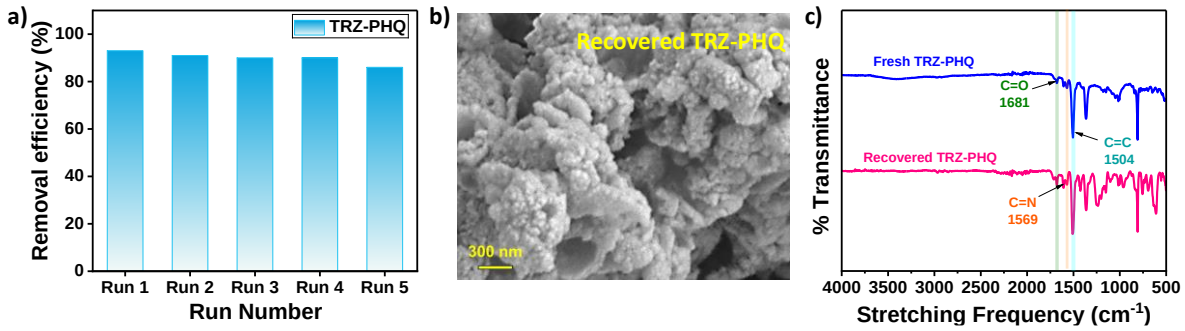

Figure S19. a) Reusability of **TRZ-PHQ** in photocatalytic degradation of CIP; b) SEM image of recovered **TRZ-PHQ** after 5th cycle; c) FTIR spectra of fresh **TRZ-PHQ** and recovered **TRZ-PHQ** after 5th cycle.

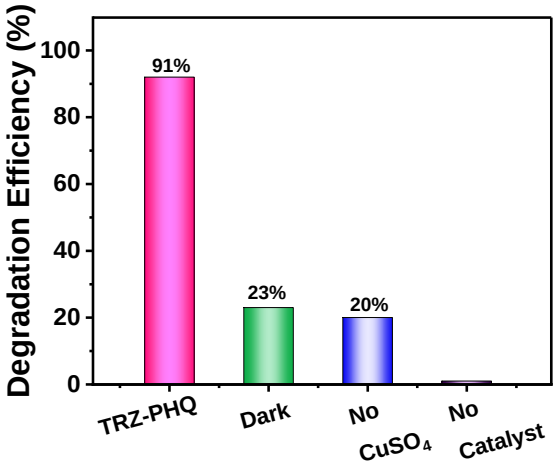

Figure S20. Control tests for photocatalytic degradation of CIP by **TRZ-PHQ**.

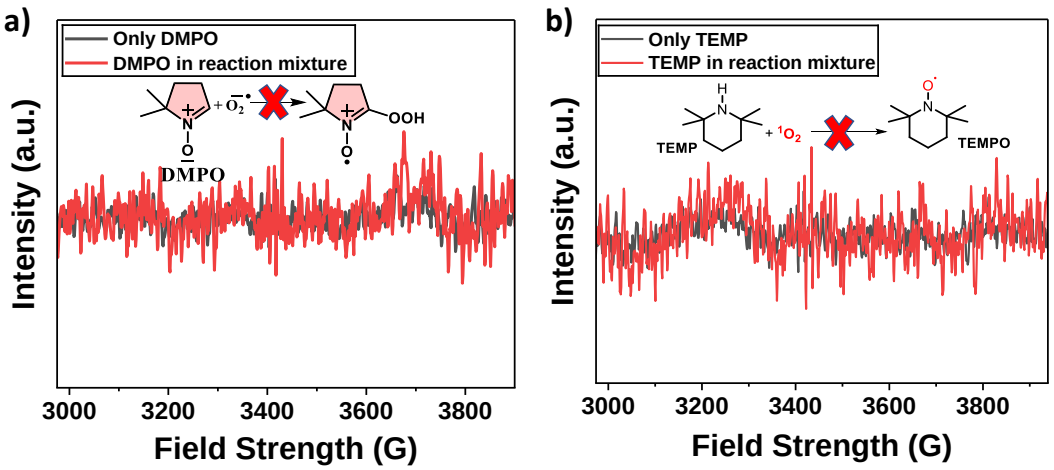

Figure S21. EPR spectra recorded using a) DMPO for $\bullet O_2^-$ trapping and b) TEMP for $^1O_2$ trapping.

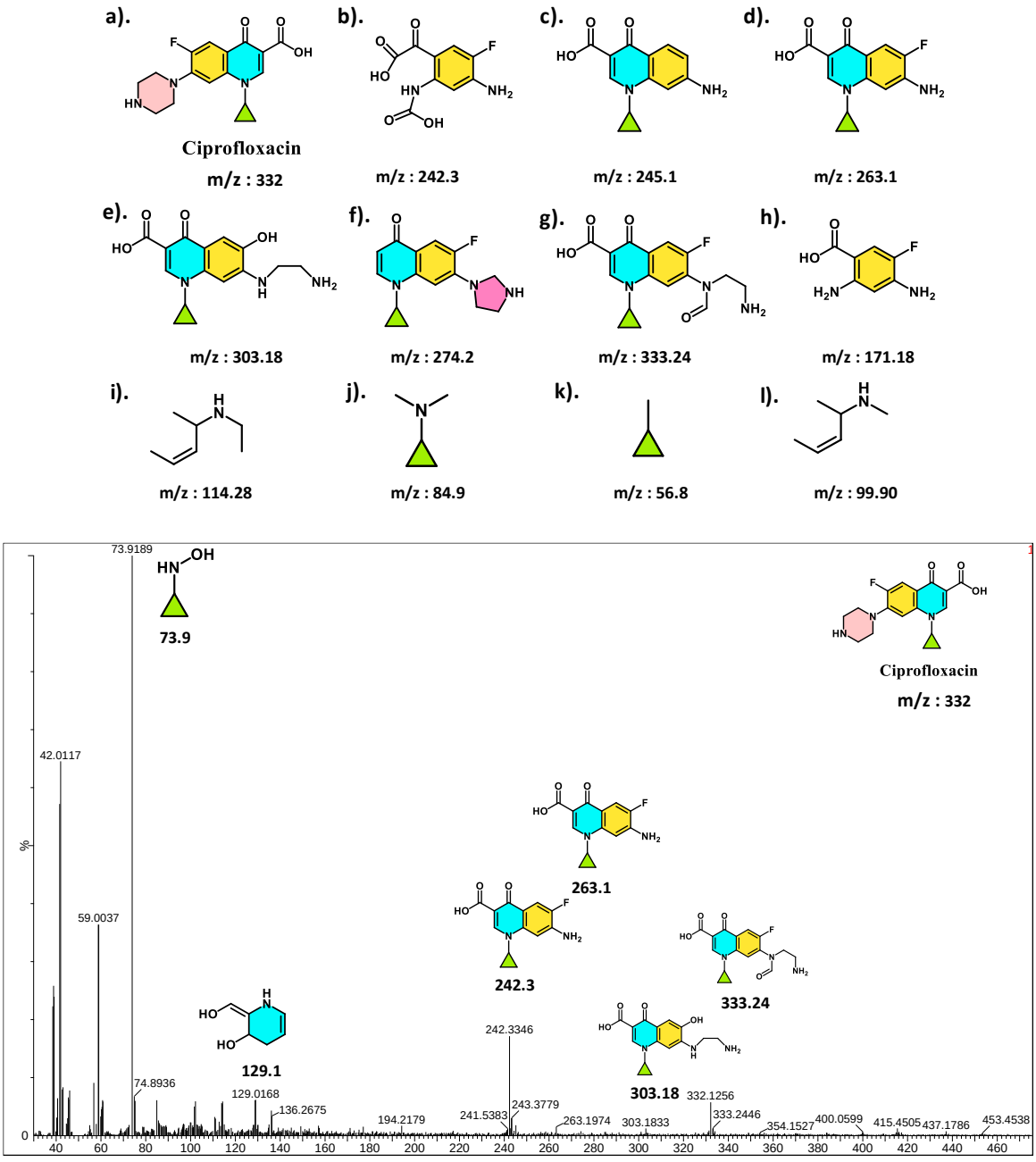

Figure S22. LC-MS spectra of CIP solutions after photodegradation by **TRZ-PHQ**.

Table S5. Comparison of Photocatalytic removal efficiencies of U(VI) on various photocatalysts.

Photocatalyst	**Solid to liquid ratio**	**Photocatalytic conditions**	**Removal time**	**Rate constant**	**U(VI) Removal efficiency**	**References**
TRZ-PHQ	0.2 g L^{-1}	CIP (50 ppm), 50 ppm	120 min	0.0175 min^{-1} (1.05 h^{-1})	95%	This work
		CIP (150 ppm), 50 ppm	30 min	0.087 min^{-1}	92 %	
ECUT-SO	0.5 g L^{-1}	Methanol, 50 ppm	60 min	0.063 min^{-1}	97.8 %	[36]
PyB-SO_3H	0.2 g L^{-1}	Methanol, 50 ppm	60 min	0.085 min^{-1}	99.2 %	[14]
PQ-TPM	0.125 g L^{-1}	Methanol, 50 ppm	180 min	0.0095 min^{-1}	80 %	[8]
TiO_2	0.4 g L^{-1}	HCOONa, 50 ppm	2.25 h	…….	96 %	[9]
g-C_3N_4	0.2 g L^{-1}	Methanol, 50 ppm	120 min	0.028 min^{-1}	96.4 %	[10]
g-C_3N_4/TiO_2	0.25 g L^{-1}	NA, 20 ppm	4 h	…….	83 %	[11]
CN550	0.2 g L^{-1}	Methanol 2mL, 326.5 ppm	390 min	0.011 min^{-1}	100 %	[12]
TT-TPP	1 g/L	200 ppm	10 h	……	97.5 %	[37]
SnS_2COF	0.5 g/L	550 ppm	120 min	0.0000684 g. mg^{-1}.min^{-1}	100 %	[16]
PyN-DAB	0.143 g/L	600 ppm	240 min	……..	98 %	[17]
BiOBr@TpPa-1	0.33 g L^{-1}	Methanol, 50 ppm	420 min	…….	76%	[18]
EUCT-AQ	0.25 g L^{-1}	Ascorbic acid, 50 ppm	120 min	0.0015 min^{-1}	86 %	[38]
CTATP-DHBA	0.25 g L^{-1}	Methanol, 200 ppm	3 h	0.0079 min^{-1}	83.27 %	[39]
Ti_3C_2/CdS	0.2 g L^{-1}	200 ppm	40 min	0.0362 min^{-1}	97 %	[13]

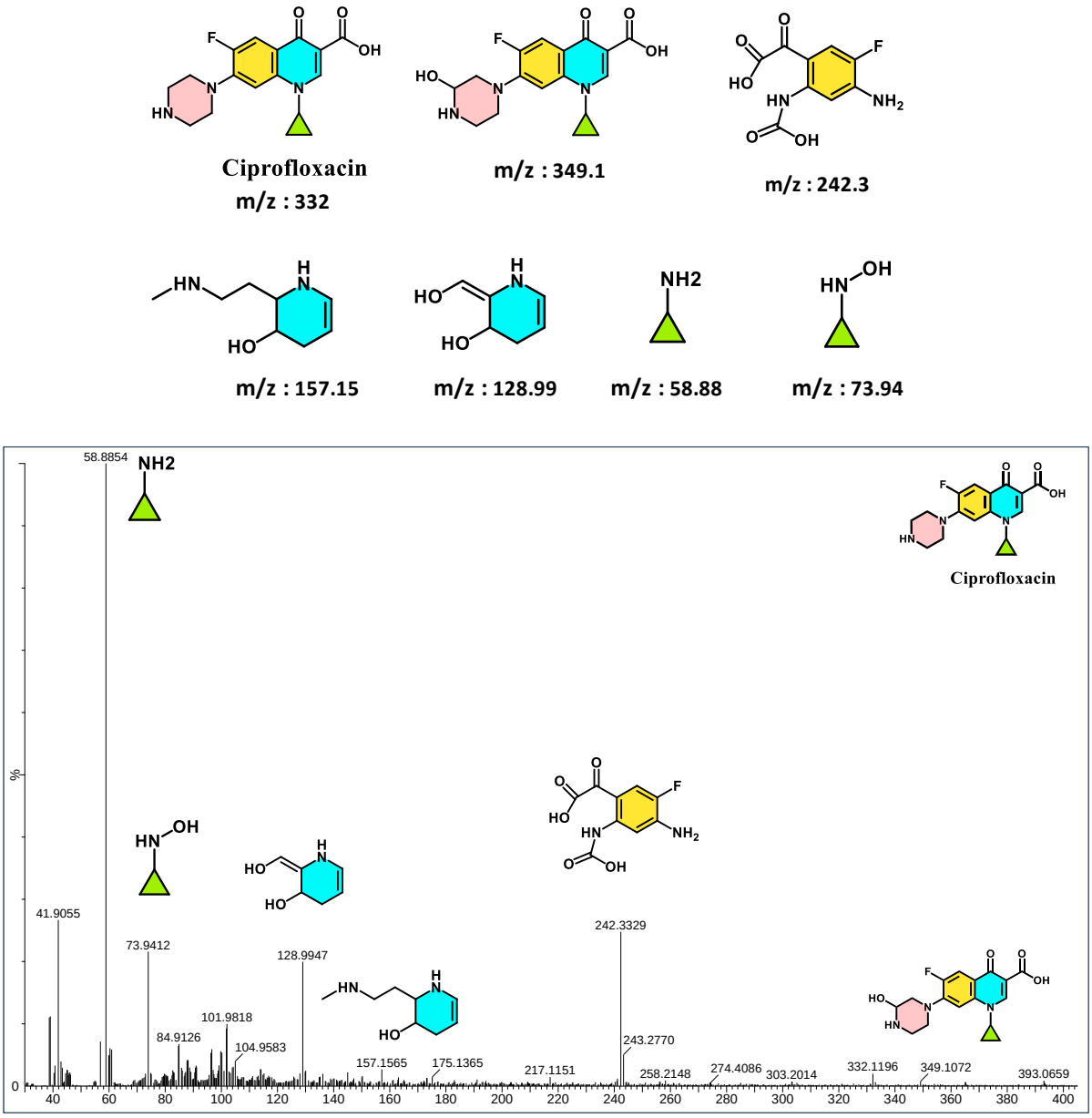

Figure S23. LC-MS spectra of CIP solutions after the simultaneous photocatalytic removal of CIP and U(VI) by **TRZ-PHQ**.

References

1. F. Banerjee, P. D. Gupta, S. Roy and S. K. Samanta, *ACS Appl. Mater. Interfaces.*, 2024, **16**, 58689-58702.
2. K. Akatsuka, G. Takanashi, Y. Ebina, M.-a. Haga and T. Sasaki, *J. Phys. Chem. C*, 2012, **116**, 12426-12433.
3. W. Zhou, J. Jia, J. Lu, L. Yang, D. Hou, G. Li and S. Chen, *Nano Energy*, 2016, **28**, 29-43.
4. H. Xu, X. Li, H. Hao, X. Dong, W. Sheng and X. Lang, *Appl. Catal. B: Environ.*, 2021, **285**, 119796.
5. S. Sau, F. Banerjee and S. K. Samanta, *ACS Appl. Nano Mater.*, 2023, **6**, 11679-11688.
6. S. Mondal, W. L. Koay, I. Daga, S. Paul, V. X. Truong and N. D. P. Singh, *J. Am. Chem. Soc.*, 2024, **146**, 23376-23386.
7. K. Maity, S. Sau, F. Banerjee and S. K. Samanta, *ACS Appl. Mater. Interfaces.*, 2024, **16**, 50834-50845.
8. Y.-R. Chen, X. Wang, X.-Y. Fan, H.-F. Wei, H.-W. Jiang, Y. Li and W.-R. Cui, *Sep. Purif. Technol.*, 2024, **334**, 126121.
9. G. Wang, J. Zhen, L. Zhou, F. Wu and N. Deng, *Journal of Radioanalytical and Nuclear Chemistry*, 2015, **304**, 579-585.
10. B. Wei, J. Luo, S. Lin, Z. Li, X. Zhu, Z. Dong, S. Xiao, X. Cao, Y. Liu and Z. Zhang, *Sep. Purif. Technol.*, 2023, **318**, 123918.
11. X.-H. Jiang, Q.-J. Xing, X.-B. Luo, F. Li, J.-P. Zou, S.-S. Liu, X. Li and X.-K. Wang, *Appl. Catal. B: Environ.*, 2018, **228**, 29-38.
12. S. Liu, Z. Wang, Y. Lu, H. Li, X. Chen, G. Wei, T. Wu, D.-J. Maguire, G. Ye and J. Chen, *Appl. Catal. B: Environ.*, 2021, **282**, 119523.
13. P. Liang, L. Yuan, K. Du, L. Wang, Z. Li, H. Deng, X. Wang, S.-Z. Luo and W. Shi, *Chem. Eng. J*, 2021, **420**, 129831.
14. F. Yu, F. Song, R. Wang, M. Xu and F. Luo, *Polymer Chemistry*, 2021, **12**, 867-875.
15. W.-R. Cui, F.-F. Li, R.-H. Xu, C.-R. Zhang, X.-R. Chen, R.-H. Yan, R.-P. Liang and J.-D. Qiu, *Angew. Chem.*, 2020, **132**, 17837-17843.
16. X. Liu, R.-X. Bi, C.-R. Zhang, Q.-X. Luo, R.-P. Liang and J.-D. Qiu, *Chem. Eng. J*, 2023, **460**, 141756.
17. C.-P. Niu, C.-R. Zhang, X. Liu, R.-P. Liang and J.-D. Qiu, *Nat. Commun.*, 2023, **14**, 4420.
18. X. Zhong, Y. Liu, S. Wang, Y. Zhu and B. Hu, *Sep. Purif. Technol.*, 2021, **279**, 119627.
19. W.-R. Cui, C.-R. Zhang, R.-H. Xu, X.-R. Chen, R.-H. Yan, W. Jiang, R.-P. Liang and J.-D. Qiu, *Small*, 2021, **17**, 2006882.
20. C.-R. Zhang, W.-R. Cui, R.-H. Xu, X.-R. Chen, W. Jiang, Y.-D. Wu, R.-H. Yan, R.-P. Liang and J.-D. Qiu, *CCS Chemistry*, 2021, **3**, 168-179.
21. H. Li, F. Zhai, D. Gui, X. Wang, C. Wu, D. Zhang, X. Dai, H. Deng, X. Su, J. Diwu, Z. Lin, Z. Chai and S. Wang, *Appl. Catal. B: Environ.*, 2019, **254**, 47-54.
22. T. Liu, A. Gu, T. Wei, M. Chen, X. Guo, S. Tang, Y. Yuan and N. Wang, *Small*, 2023, **19**, 2208002.
23. H. Zhang, W. Liu, A. Li, D. Zhang, X. Li, F. Zhai, L. Chen, L. Chen, Y. Wang and S. Wang, *Angew. Chem., Int. Ed.*, 2019, **58**, 16110-16114.
24. M. Qiu, Z. Liu, S. Wang and B. Hu, *Environ. Res.*, 2021, **196**, 110349.
25. K. K. Das, S. Patnaik, S. Mansingh, A. Behera, A. Mohanty, C. Acharya and K. M. Parida, *J. Colloid Interface Sci.*, 2020, **561**, 551-567.
26. C. Chuaicham, R. R. Pawar, S. Karthikeyan, B. Ohtani and K. Sasaki, *J. Colloid Interface Sci.*, 2020, **577**, 397-405.
27. M. Zhou, L. Jing, M. Dong, Y. Lan, Y. Xu, W. Wei, D. Wang, Z. Xue, D. Jiang and J. Xie, *Chemosphere*, 2021, **268**, 128839.
28. C. Chuaicham, K. Sekar, Y. Xiong, V. Balakumar, Y. Mittraphab, K. Shimizu, B. Ohtani, I. Dabo and K. Sasaki, *Chem. Eng. J*, 2021, **425**, 130502.
29. F. Nekouei, S. Nekouei, M. Pouzesh and Y. Liu, *Chem. Eng. J*, 2020, **385**, 123710.

30.Y. Pan, X. Hu, D. Shen, Z. Li, R. Chen, Y. Li, J. Lu and M. Bao, *Sep. Purif. Technol.*, 2022, **295**, 121216.
31.N. Lu, P. Wang, Y. Su, H. Yu, N. Liu and X. Quan, *Chemosphere*, 2019, **215**, 444-453.
32.N. Liu, N. Lu, Y. Su, P. Wang and X. Quan, *Sep. Purif. Technol.*, 2019, **211**, 782-789.
33.X. Li, Y. Qiu, Z. Zhu, T. Chen, H. Zhang and D. Yin, *Chem. Eng. J*, 2022, **440**, 135840.
34.M. Zhang, C. Lai, B. Li, D. Huang, G. Zeng, P. Xu, L. Qin, S. Liu, X. Liu, H. Yi, M. Li, C. Chu and Z. Chen, *J. Catal.*, 2019, **369**, 469-481.
35.M. Zhang, Y. Zhang, Y. Zhu, J. Wang, L. Qiao, Y. Zhao, Y. Tao, Y. Xiao and L. Tang, *Chem. Eng. J*, 2023, **464**, 142533.
36.F. Yu, Z. Zhu, S. Wang, Y. Peng, Z. Xu, Y. Tao, J. Xiong, Q. Fan and F. Luo, *Chem. Eng. J*, 2021, **412**, 127558.
37.L. Chen, B. Chen, J. Kang, Z. Yan, Y. Jin, H. Yan, S. Chen and C. Xia, *Chem. Eng. J*, 2022, **431**, 133222.
38.F. Yu, Z. Zhu, C. Li, W. Li, R. Liang, S. Yu, Z. Xu, F. Song, Q. Ren and Z. Zhang, *Appl. Catal. B: Environ.*, 2022, **314**, 121467.
39.X. Wang, W. Xu and W.-R. Cui, *J. Hazard. Mater.*, 2024, **463**, 132846.